Phytochemistry 170 (2020) 112216

Contents lists available at ScienceDirect

Phytochemistry

journal homepage: www.elsevier.com/locate/phytochem

Hyperelodiones A-C, monoterpenoid polyprenylated acylphloroglucinols from *Hypericum elodeoides*, induce cancer cells apoptosis by targeting RXRα

Daren Qiu[1], Mi Zhou[1], Junjie Chen, Guanghui Wang, Ting Lin, Yujie Huang, Furong Yu, Rong Ding, Cuiling Sun, Wenjing Tian**, Haifeng Chen*

Fujian Provincial Key Laboratory of Innovative Drug Target Research, School of Pharmaceutical Sciences, Xiamen University, Xiamen 361005, China

ARTICLE INFO

Keywords:
Hypericum elodeoides choisy
Hyperelodiones
MCF-7 cell
HeLa cell
RXRα

ABSTRACT

Hyperelodiones A-C, three undescribed monoterpenoid polyprenylated acylphloroglucinols possessing 6/6/6 fused tricyclic core, were isolated from *Hypericum elodeoides* Choisy. Their gross structures were elucidated by HRESIMS and NMR data. The absolute configurations of hyperelodiones A-C were assigned by their calculated and compared electronic circular dichroism (ECD) spectra combined with their common biosynthetic origin. A fluorescence quenching assay suggested that hyperelodiones A-C could bind to RXRα-LBD, whereas hyperelodione C showed the strongest interaction with a K_D of 12.81 μM. In addition, hyperelodiones A-C dose-dependently inhibited RXRα transactivation and the growth of HeLa and MCF-7 cells. Among them, hyperelodione C showed the most potent inhibitory activities and dose-dependent PARP cleavage. Molecular docking results suggested that hyperelodione C showed a different interaction mode compared with hyperelodione A and hyperelodione B. Thus, hyperelodione C can be considered as a promising lead compound for cancer therapy, which can bind to RXRα-LBD and induce HeLa and MCF-7 cell apoptosis.

1. Introduction

Polycyclic polyprenylated acylphloroglucinols (PPAPs) are a class of structurally fascinating natural products that possess highly oxygenated acylphloroglucinol-derived cores. Prenylation of this core moiety affords monocyclic polyprenylated acylphloroglucinols (MPAPs), which are further cyclized to various types of PPAP metabolites (Ciochina and Grossman, 2006). Monoterpenoid polyprenylated acylphloroglucinols, generally decorated with a geranyl or a cyclic monoterpene fragment at C-3 of the phloroglucinol ring are ascribed to the MPAP family (Li et al., 2019). Apart from their intriguing chemical structures, PPAPs have been reported to show diverse activities, such as anticancer, anti-inflammatory, anti-HIV, antiplasmodial, and antimicrobial activities (Decosterd et al., 1989; Fobofou et al., 2015; Yang et al., 2015; Zhang et al., 2015; Zhu et al., 2015). However, the mechanism of action of PPAPs still need further investigation. The retinoid X receptor α (RXRα), a ligand-dependent transcriptional factor, has multiple physiological functions including cell proliferation, differentiation, and apoptosis (Robinsonrechavi et al., 2003). RXRα is an ideal drug target for cancer therapy, and its ligand Targretin has been approved by the FDA for the treatment of cutaneous T-cell lymphoma (Lenhard et al., 1999). Our previous research has shown that several PPAPs exhibit RXRα transcriptional inhibitory activities, while some PPAPs have shown a direct interaction with the ligand-binding domain (LBD) of RXRα (Tian et al., 2014a, 2014c, 2016, 2017a, 2017b).

The majority of PPAPs have been reported to be isolated from the plants of family Guttiferae (Clusiaceae), especially from the genera *Hypericum* and *Garcinia* (Yang et al., 2018). To identify more undescribed PPAPs as small-molecule regulators of RXRα, a phytochemical study of *Hypericum elodeoides* Choisy was carried out. As a result, three undescribed monoterpenoid polyprenylated acylphloroglucinols (**1–3**) possessing 6/6/6 fused tricyclic core were obtained, of which **3** could bind to RXRα-LBD and induce HeLa and MCF-7 cell apoptosis. The monoterpenoid fragments in **1–3** have been predicted to be biosynthesized by an isopentenyl at C-3, forming a dihydropyran ring with the 4-OH of the core structure, with another lateral prenyl group located at C-8 cyclizing into a six-membered ring by a carbon–carbon bond formation between C-5 and C-7, which is quite different from the reported monoterpenoid polyprenylated acylphloroglucinols cyclized by a geranyl group (two prenyl groups linked from head to tail) at C-3.

* Corresponding author.
** Corresponding author.
E-mail addresses: tianwj@xmu.edu.cn (W. Tian), haifeng@xmu.edu.cn (H. Chen).
[1] These two authors contributed equally to this research.

https://doi.org/10.1016/j.phytochem.2019.112216
Received 1 September 2019; Received in revised form 18 November 2019; Accepted 20 November 2019
Available online 14 December 2019
0031-9422/

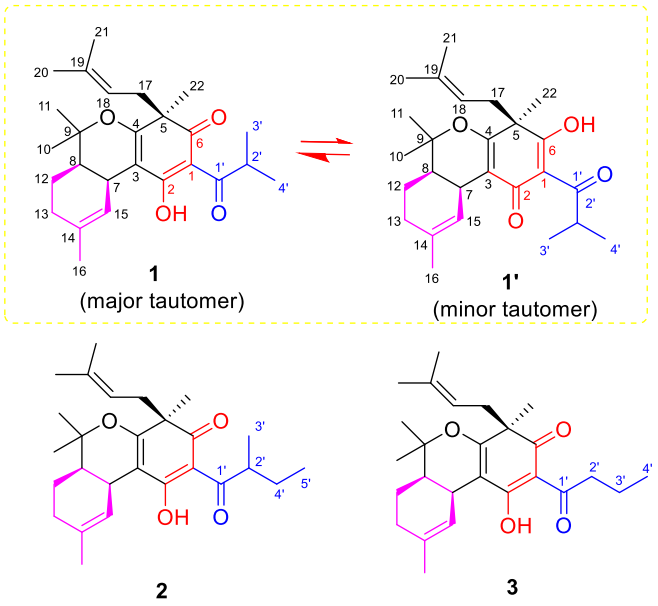

Fig. 1. Structure of compounds 1–3.

In this paper, the isolation, structural elucidation and biological activity evaluation of these three undescribed monoterpenoid polyprenylated acylphloroglucinols (**1–3**) will be reported.

2. Results and discussion

2.1. Isolation and structural elucidation

The dried whole plants of *H. elodeoides* (12.9 kg) were extracted exhaustively with 95% aqueous EtOH and partitioned consecutively with petroleum ether. The fluorescence quenching assay suggested that the EtOH and petroleum ether extracts could bind to RXRα with a K_D values of 56.37 μM and 42.09 μM, respectively (supporting information). Thus, the petroleum ether extract was further studied to identify the small-molecule regulators of RXRα. As a result, through various column chromatography and reversed-phase HPLC procedures, three undescribed active compounds (**1–3**) were obtained (Fig. 1).

Hyperelodione A (**1**) was obtained as a yellowish oil and assigned the molecular formula $C_{26}H_{36}O_4$ on the basis of the HRESIMS $[M+H]^+$ ion at *m/z* 413.2695 $[M+H]^+$ (calcd. for $C_{26}H_{37}O_4$, 413.2686), corresponding to nine indices of hydrogen deficiency. The IR (1651 cm^{-1} and 3581 cm^{-1}) spectrum indicated the presence of carbonyl and hydroxyl groups. The ^{13}C NMR and DEPT-135 data of compound **1** (Table 1) showed 26 carbon signals, including an isopropyl group [δ_C 35.4 (C-2′), 19.0 (C-3′), 19.4 (C-4′)], an isopentenyl group [δ_C 35.7 (C-17), 120.3 (C-18), 133.6 (C-19), 25.9 (C-20), 18.3 (C-21)], an enol-*β*-triketone group [δ_C 106.2 (C-1), 190.1 (C-2), 196.4 (C-6), and 207.2 (C-1′)], an enol group [δ_C 170.3 (C-4), 107.9 (C-3)], together with two olefinic carbons [δ_C 134.9 (C-14), 121.6 (C-15)], four methyls [δ_C 25.83 (Me-10), 25.1 (Me-11), 23.8 (Me-16), 25.78 (Me-22)], two methylenes [δ_C 19.9 (C-12), 30.1 (C-13)], two methines [δ_C 30.3 (C-7), 40.0 (C-8)] and one quaternary carbon [δ_C 80.0 (C-9)], which accounted for six indices of hydrogen deficiency. The remaining three indices of hydrogen deficiency required tricyclic structure in **1**. The above analyses implied that **1** was a derivative of acylphloroglucinol. In the HMBC spectrum, the correlations from the active proton of OH-2 (δ_H 19.34) to C-1 (δc 106.2), C-2 (δc 190.1), C-1′ (δc 207.2), and C-2′ (δc 35.4) confirmed the existence of the enol-*β*-triketone group and located the position of the OH group at C-2. It also indicated that a pseudo six-membered heterocyclic ring was formed due to strong intramolecular hydrogen bonding between the active hydrogen and O-2′.

Table 1
NMR spectroscopic data for 1–3 (600 MHz, $CDCl_3$).

No.	1		2		3	
	δ_C, type	δ_H (*J* in Hz)	δ_C, type	δ_H (*J* in Hz)	δ_C, type	δ_H (*J* in Hz)
1	106.2, C		106.7, C		107.2, C	
2	190.1, C		190.2, C		189.9, C	
3	107.9, C		107.9, C		107.8, C	
4	170.3, C		170.2, C		170.4, C	
5	53.2, C		53.1, C		53.0, C	
6	196.4, C		196.5, C		196.6, C	
7	30.3, CH	3.28, br.s	30.3, CH	3.28, br.s	30.3, CH	3.28, br.s
8	40.0, CH	1.67, m	40.0, CH	1.68, m	40.0, CH	1.66, m
9	80.0, C		80.0, C		80.0, C	
10	25.83, CH_3	1.40, s	25.75, CH_3	1.40, s	25.84, CH_3	1.41, s
11	25.1, CH_3	1.26, s	25.2, CH_3	1.26, s	25.1, CH_3	1.27, s
12	19.9, CH_2	1.80, m 1.25, m	20.0, CH_2	1.81, m 1.26, m	19.9, CH_2	1.80, m 1.23, m
13	30.1, CH_2	1.98, m 1.89, dd (4.8, 12.0)	30.1, CH_2	1.98, m 1.90, m	30.1, CH_2	1.97, m 1.90, dd (4.8, 12.0)
14	134.9, C		134.8, C		134.9, C	
15	121.6, CH	6.09, d (3.0)	121.7, CH	6.09, s	121.6, CH	6.09, d (4.8)
16	23.8, CH_3	1.67, s	23.8, CH_3	1.68, s	23.8, CH_3	1.67, s
17	35.7, CH_2	2.71, dd (5.4, 8.4) 2.49, dd (4.8, 9.0)	35.9, CH_2	2.70, dd (6.6, 7.8) 2.49, m	35.8, CH_2	2.71, dd (4.8, 9.0) 2.50, dd (4.8, 9.0)
18	120.3, CH	4.77, m	120.2, CH	4.77, m	120.2, CH	4.76, m
19	133.6, C		133.6, C		133.6, C	
20	25.9, CH_3	1.53, s	25.9, CH_3	1.54, s	25.84, CH_3	1.54, s
21	18.3, CH_3	1.59, s	18.3, CH_3	1.59, s	18.3, CH_3	1.60, s
22	25.78, CH_3	1.25, s	25.66, CH_3	1.25, s	25.80, CH_3	1.25, s
1′	207.2, C		206.8, C		202.8, C	
2′	35.4, CH	3.97, sept (6.6, 7.2)	41.7, CH	3.83, m	41.7, CH	2.97, m
3′	19.0, CH_3	1.11, d (6.6)	16.4, CH_3	1.09, d (6.6)	18.9, CH_3	1.66, m
4′	19.4, CH_3	1.17, d (6.6)	27.0, CH_2	1.80, m	14.3, CH_3	1.00, t (7.2)
5′			12.0, CH_3	0.96, t (7.8)		

The correlations from δ_H 1.25 (H_3-22) to δ_C 170.2 (C-4), 53.1 (C-5), and 196.5 (C-6), together with those from δ_H 3.28 (H-7) to δ_C 107.9 (C-3) and 170.2 (C-4) indicated the linkage of C3/C4/C5/C6. In addition, the HMBC correlations from δ_H 1.11 (Me-3′)/1.17 (Me-4′) to δ_C 35.4 (C-2′) and 207.2 (C-1′) suggested that isopropyl group was linked to C-1′ of the enol-*β*-triketone group. Thus, a methylated acylphloroglucinol core was deduced. Furthermore, the HMBC correlations from δ_H 2.71, 2.49 (H_2-17) to C-5, C-18, and C-19 suggested the linkage of isoprenyl groups to C-5 of the core structure. In addition, the ^1H–^1H COSY correlations of δ_H 6.09 (H-15)/3.28 (H-7), δ_H 3.28 (H-7)/1.67 (H-8), δ_H 1.67 (H-8)/1.25 (H_a-12), and δ_H 1.25 (H_a-12)/1.98, 1.89 (H_2-13) showed a long spin system arising from the C-15 − C-7 − C-8 − C-12 partial structure. Combined with the HMBC correlations from H-7 to C-3/C-6/C-4/C-8/C-12, H-8 to C-3/C-15, H_3-10/H_3-11 to C-9, H_2-13 to C-8/C-14/C-15, and H_3-16 to C-13/C-14/C-15 indicated that an isopentenyl at C-3 formed a dihydropyran ring with the 4-OH of the core structure and another lateral prenyl group located at C-8 cyclized to form a six-membered ring by a carbon–carbon bond formed between C-15 and C-7 (Fig. 2). Hence, the 2D structure of **1** was deduced.

In the NOESY spectrum of **1**, the correlations between δ_H 3.28 (H-7) and 1.26 (H_3-11) indicated that H-7 and Me-11 were located at the axial position with the same orientation. In addition, the NOESY correlations of δ_H 1.67 (H-8)/1.26 (H_3-11), and δ_H 1.67 (H-8)/1.40 (H_3-10) further suggested that the cyclohexene moiety was *cis*-fused with the dihydropyran ring. Moreover, the NOESY correlations of δ_H 1.40 (H_3-10)/

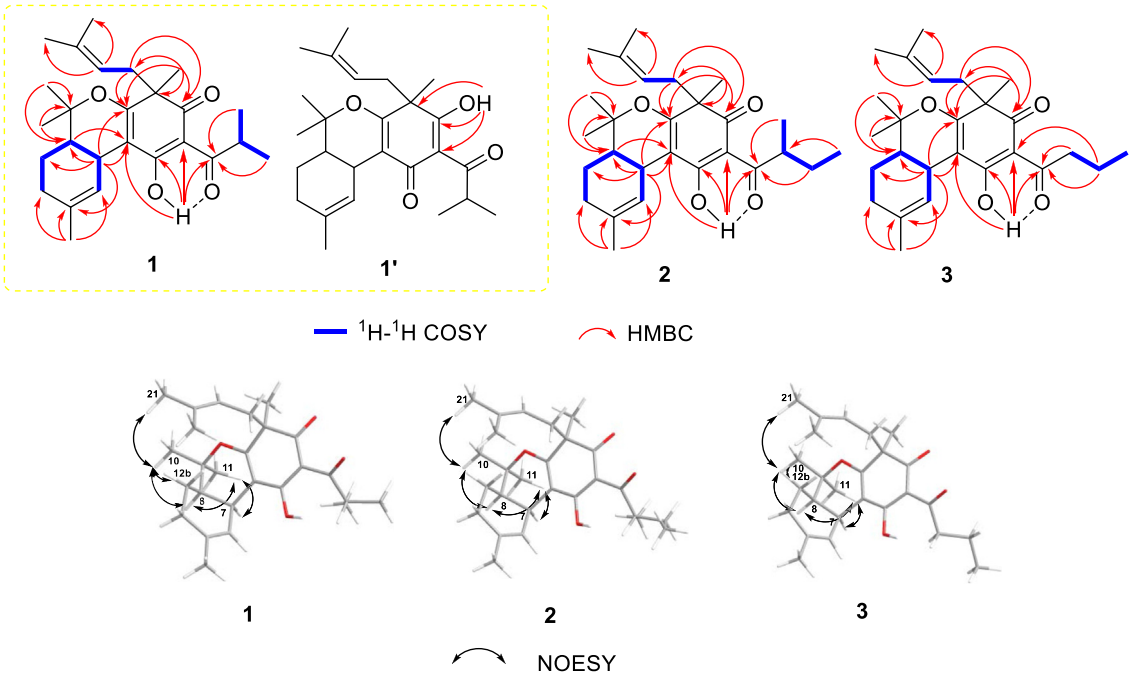

Fig. 2. Key HMBC, ^{1}H–^{1}H COSY and NOESY correlations of compounds 1–3.

1.59 (H_3-21) and δ_H 1.40 (H_3-10)/1.80 (H_b-12) suggested the same orientation of Me-10 and the isoprenyl group at C-5 (Fig. 2).

There was the presence of another minor tautomer (**1′**) due to the keto-enol tautomerism of the enol-*β*-triketone moiety. The NMR data of **1′** were similar to **1**, except for the location of the OH group. In the HMBC spectrum of **1′**, the active proton (δ_H 18.39) was correlated to C-1 (δc 110.4), C-5 (δc 47.8), and C-6 (δ_C 197.3), which located the position of the OH group at C-6. Due to the phenomenon of keto-enol tautomerism, the NMR data of **1** were recorded in different solvents, including $CDCl_3$, CD_3OD, acetone-d_6, DMSO-d_6, and acetonitrile-d_3. As a result, the ratios of the two tautomers (**1**: **1′**) were approximately 1:0.23, 1:0.28, 1:0.17, 1:0.20 and 1:0.17 in the $CDCl_3$, CD_3OD, acetone-d_6, DMSO-d_6, and acetonitrile-d_3, respectively (supporting information). The ratio of the major tautomer (**1**) was larger in acetone-d_6, DMSO-d_6 and acetonitrile-d_3 than in $CDCl_3$ and CD_3OD. The ECD curve of **1** was recorded in acetonitrile, the tautomer (**1**) was the main component. The absolute configurations of **1** were assigned by comparison of the experimental and the calculated electronic circular dichroism (ECD) spectra. Due to the presence of minor tautomer (**1′**), the theoretical ECD calculation was conducted in acetonitrile using time-dependent density functional theory (TD-DFT) at the B3LYP/6–31 + g (d, p) level for the low energy conformers of the two tautomers (5*R*,7*S*,8*R*)-**1** and (5*R*,7*S*,8*R*)-**1′**. The ECD spectrum of (5*R*,7*S*,8*R*)-**1** and fitted ECD curve of two tautomers [(5*R*,7*S*,8*R*)-**1** and (5*R*,7*S*,8*R*)-**1′**] were generated using the program SpecDis 1.6 (University of Würzburg, Würzburg, Germany) and GraphPad Prism 5 (University of California San Diego, USA) from dipole-length rotational strengths by applying Gaussian band shapes with sigma = 0.3 eV. As a result, the overall experimental ECD curve of **1** matched well with the calculated ECD spectrum of (5*R*,7*S*,8*R*)-**1** as well as the fitted spectrum of two tautomers [(5*R*,7*S*,8*R*)-**1** and (5*R*,7*S*,8*R*)-**1′**] (Fig. 3). Thus, the minor tautomer contributed slightly to the ECD spectrum of **1**. Consequently, the absolute configurations of **1** were assigned as 5*R*,7*S*,8*R*.

Hyperelodione B (**2**) was isolated as a yellowish oil with the molecular formula $C_{27}H_{38}O_4$ revealed by its HRESIMS $[M+H]^+$ ion signal at m/z 427.2846 $[M+H]^+$ (calcd. for $C_{27}H_{39}O_4$, 427.2843), requiring nine indices of hydrogen deficiency. The IR spectrum of **2** (1656, 3631 cm^{-1}) indicated the presence of carbonyl and hydroxyl groups.

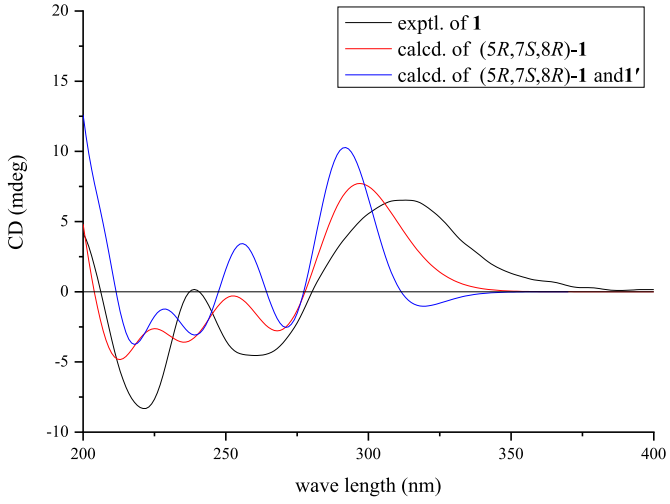

Fig. 3. Calculated and experimental ECD spectra of 1 and two tautomers.

The ^{13}C NMR data of **2** were similar to those of **1** except for the isopropyl group was replaced by a *sec*-butyl group in **2**, as assigned by the HMBC correlations from δ_H 1.09 (Me-3′) to δ_C 206.8 (C-1′)/δ_C 41.7 (C-2′)/δ_C 27.0 (C-4′) and from δ_H 0.96 (Me-5′) to C-2′/C-4′ (Fig. 2). Thus, the 2D structure of **2** was elucidated. The NOESY correlations of **2** were similar to **1**, which resulted in the same relative configuration (Fig. 2). The absolute configuration of the chiral center in the *α*-methylbutyryl group can be determined on the basis of optical rotation data by the means of Brewster's rule of atomic asymmetry (Pei et al., 1989). According to this rule, if the absolute configuration of the chiral center in the *α*-methylbutyryl group is *S*, the optical value will be dextrorotation (+). The optical rotation value of **2** ($[\alpha]_D^{28}$ +26.3) was opposite that of **1** ($[\alpha]_D^{28}$–18.6), which assigned the absolute configuration of C-2′ as *S*. Furthermore, the absolute configuration of the *α*-methylbutyryl group in the reported analogues hyperjapone C and E from the same genus were unambiguously determined as *S* by the X-ray analysis (Yang et al., 2016). Thus, based on the biogenesis relationship, the absolute configuration of C-2′ can be further confirmed as *S*. Moreover, the

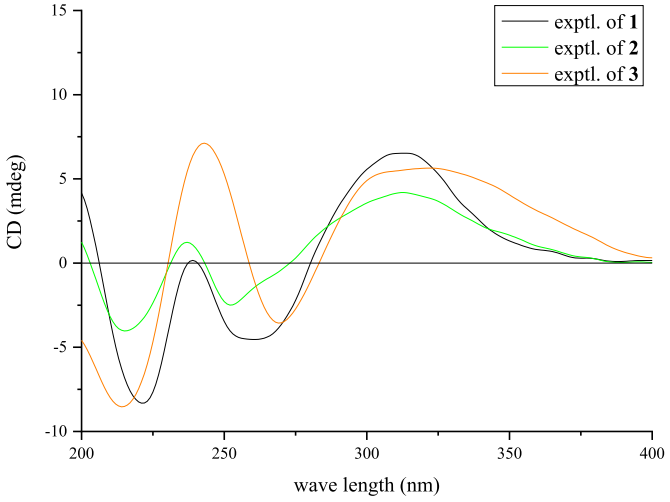

Fig. 4. Experimental ECD spectra of 1–3.

experimental ECD data of **2** had a high degree of similarity to that of the biogenetically related **1** (Fig. 3). Another minor tautomer with an OH group at C-6 also existed for **2**, which contributed little influence on the CD spectrum of **2** (Fig. 4). Thus, the absolute configurations of the chiral carbons in **2** were defined as 2′*S*,5*R*,7*S*,8*R*.

Hyperelodione C (**3**), a yellowish oil, was assigned the molecular formula of $C_{26}H_{36}O_4$ via ^{13}C NMR and HRESIMS data with an $[M+H]^+$ ion at m/z 413.2678 (calcd. for $C_{26}H_{37}O_4$, 413.2686), which accounted for nine indices of hydrogen deficiency. The IR absorptions at 3449 and 1651 cm^{-1} also indicated the presence of carbonyl and hydroxyl groups. The ^{13}C NMR data of **3** were identical to those of **1** except for an *n*-propyl group substituent at C-1′ instead of an isopropyl group, which was further confirmed by the HMBC and ^1H–^1H COSY data (Fig. 2). The relative configuration of **3** was also determined by the NOESY correlations, which resulted in the same configuration as that of **1** and **2** (Fig. 2). There was also another minor tautomer with the OH group at C-6 as in **1** and **2**, which slightly influenced the CD curve. The experimental ECD data of **3** well to that of the biogenetically related **1** (Fig. 4), which allowed the assignment of the same absolute configuration of 5*R*,7*S*,8*R*.

The putative biogenetic pathway of **1–3** was proposed (Scheme 1). The structures of **1–3** were proposed to derive from the isobutyryl-CoA (**i**), α-methylbutyryl-CoA (**ii**), and butyryl-CoA (**iii**), respectively. Then, further condensation with three malonyl-CoAs formed the acylphloroglucinol core through the represented polyketide-type biosynthesis pathway (Abe et al., 2004). The acylphloroglucinol core was further prenylated and methylated to afford monocyclic polyprenylated acylphloroglucinols (MPAPs) (Ciochina and Grossman, 2006). Finally, compounds **1–3** were putatively biosynthesized from MPAPs through a series of reactions involving epoxidation, intramolecular cyclization, dehydration and reduction (Hu et al., 2000; Tian et al., 2014b).

2.2. The interaction between RXRα-LBD and compounds 1–3

RXRα, a crucial member of the nuclear receptor superfamily, is a ligand-dependent transcription factor. RXRα regulates biological processes such as cell differentiation, proliferation and apoptosis through the interaction with small-molecule modulators. RXRα possesses the classical functional domains of nuclear receptors, including a DNA-binding domain (DBD) and a ligand-binding domain (LBD) (Altucci et al., 2007). Many natural products have been demonstrated to bind to the RXRα-LBD to modulate the genomic or nongenomic function of RXRα. In this study, the interactions between the RXRα-LBD and the compounds were investigated by fluorescence quenching technology, a method that measures the fluorescence quenching caused by a ligand binding to the protein. Gradual fluorescence quenching was observed when RXRα-LBD was exposed to increasing concentration of the new compounds **1–3** (Fig. 5). The results showed that the binding constants (K_D values) of compounds **1** and **2** to the RXRα-LBD were fitted as 47.01 μM and 32.50 μM, respectively, while compound **3** could bind to RXRα-LBD with a K_D of 12.81 μM. These data indicated that compounds **1–3** have the potential to bind to RXRα, while compound **3** showed a stronger interaction with the RXRα-LBD than the other two compounds.

2.3. The RXRα transactivation effects of compounds 1–3

As a nuclear receptor, RXRα has genomic functions via transactivation. The effects of compounds **1–3** on RXRα transactivation were examined by dual-luciferase reporter gene assay. As shown in Fig. 5, all the compounds inhibited 9-*cis*-RA-induced RXRα transactivation at concentrations of 12.5 μM and 25 μM, while compound **3** exhibited

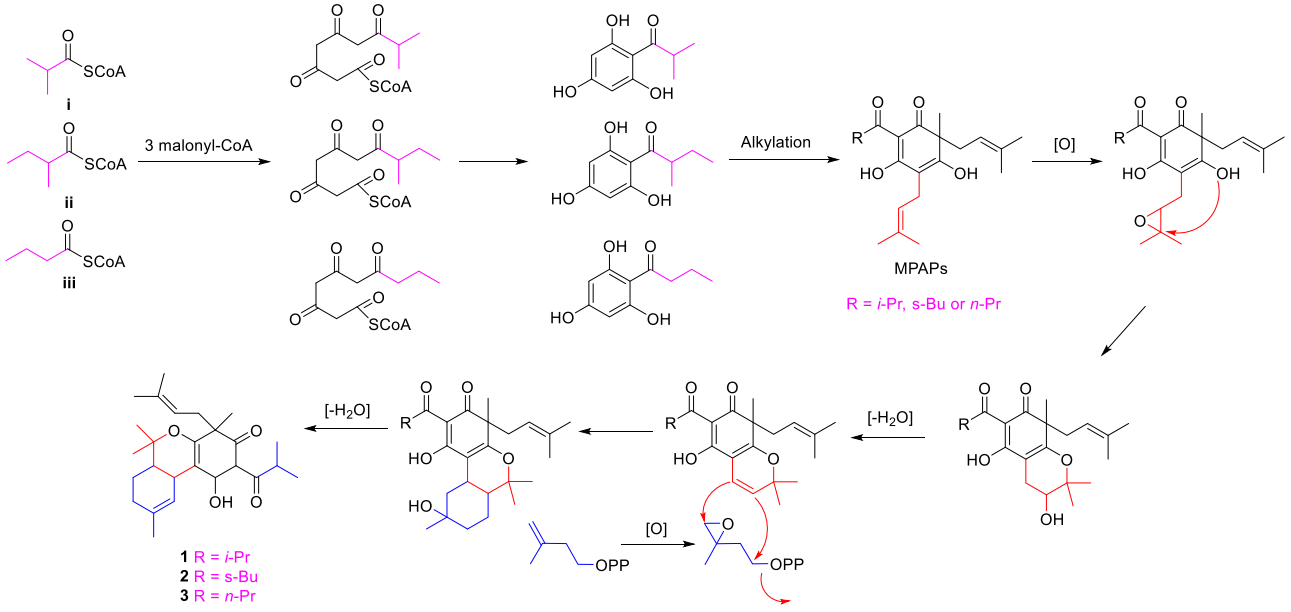

Scheme 1. Plausible Biogenetic Pathway of 1–3.

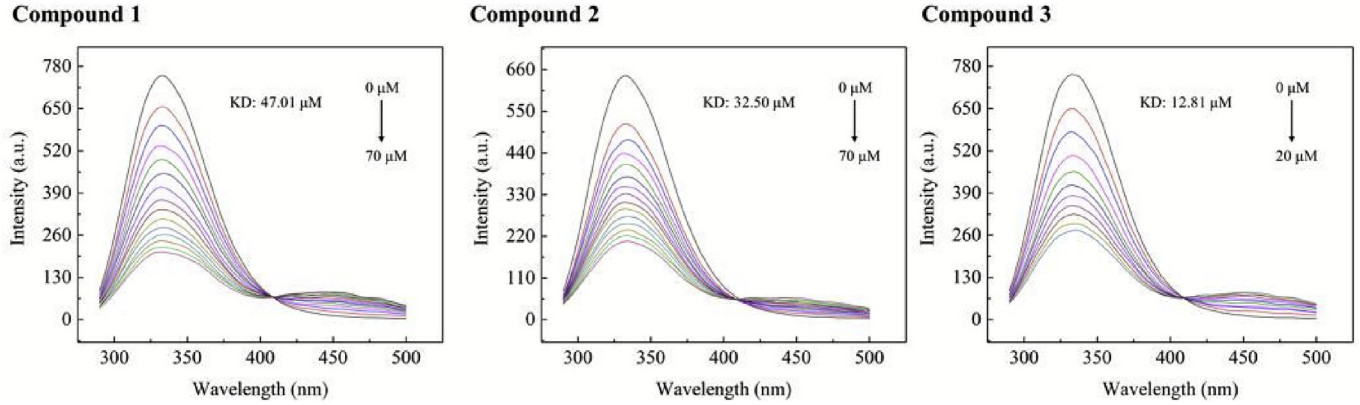

Fig. 5. The interaction between RXRα-LBD and compounds. After treated with compounds 1–3, the binding affinity of compound toward RXRα-LBD was measured via fluorescence quenching technology at 298 K.

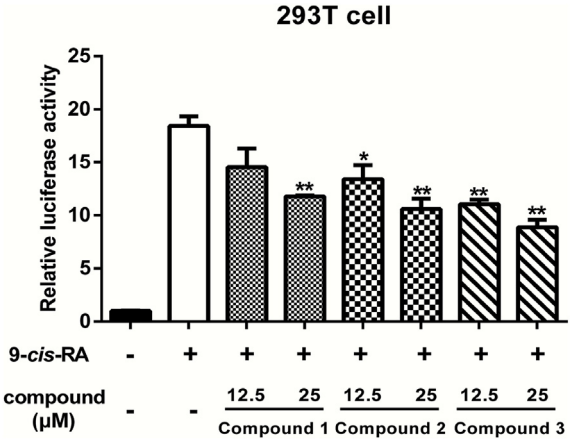

Fig. 6. The RXRα transactivation effects of compounds. 293T cells were treated with different concentrations of new compounds (0, 12.5, 25 μM), the transactivation activities of reporter gene for RXRα were measured by dual-luciferase reporter gene assay. The values are the mean ± SD for four independent replicates (*p < 0.05, **p < 0.01, compared with cells treated with 9-*cis*-RA alone).

better inhibitory activity than the other two compounds at the same concentrations (Fig. 6).

2.4. Growth inhibitory activities of compounds *1–3* on MCF-7 and HeLa cells

The growth inhibitory effects of compounds **1–3** on the human cervical cancer cell line (HeLa) and human breast cancer cell line (MCF-7) were examined. As a result, all the compounds exhibited cytotoxic effects on these two cancer cell lines in a dose-dependent manner (Fig. 7). Among them, compound **3** showed the most potent growth inhibitory effects on the HeLa and MCF-7 cell lines with IC50 values of 24.39 and 26.33 μM, respectively, while the IC50 values of compound **1** on these two cancer cells were 37.80 and 44.37 μM, and the IC50 values of compound **2** were 51.44 and 61.66 μM, respectively. The above data suggested that compound **3** displayed potent anti-proliferative activity against HeLa and MCF-7 cells, while compounds **1** and **2** had moderate cytotoxic activities.

2.5. Induction of PARP cleavage by compound *3*

To investigate whether compound **3** induces cancer cell apoptosis, HeLa and MCF-7 cells were incubated with increasing concentrations (10–30 μM) of compound **3** for 48 h. Cleaved poly (ADP-ribose)

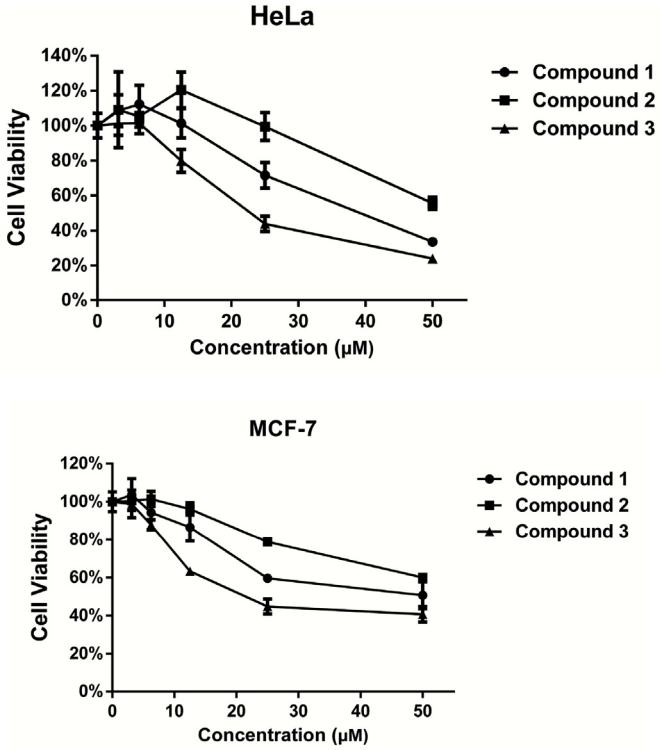

Fig. 7. Cytotoxic effects of compounds 1–3. HeLa and MCF-7 cells were exposed to various concentrations of compounds 1–3 (0, 3.125, 6.25, 12.5, 25, 50 μM). After 48 h, cytotoxic activities of compounds against cancer cells were measured by MTT assay. The values are the mean ± SD for four independent replicates.

polymerase (PARP), a typical apoptotic marker in the apoptotic response, was measured via Western blot. As a result, **3** induced HeLa and MCF-7 cell apoptosis with a dose dependent PARP cleavage (Fig. 8). Thus, compound **3** could potentially induce HeLa cells and MCF-7 cell apoptosis.

2.6. Molecular docking of *1–3* to RXRα-LBD

Molecular docking is an effective way to preliminarily understand the structure-activity relationship (SAR) by exploring the interaction mode between a compound and the targeted protein. In this study, a molecular docking technique was used to predict the interaction between compounds **1–3** and the RXRα-LBD protein with Molecular Operating Environment (MOE) (2009.10) software. As a result, the

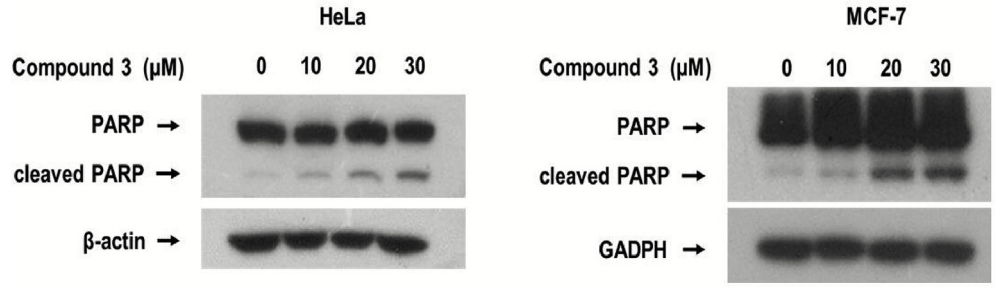

Fig. 8. PARP cleavage induction by compound 3. HeLa cells and MCF-7 cells were treated with different concentrations of compound 3 (0, 10, 20, 30 μM) for 48 h. The level of cleaved PARP was analyzed by Western blot.

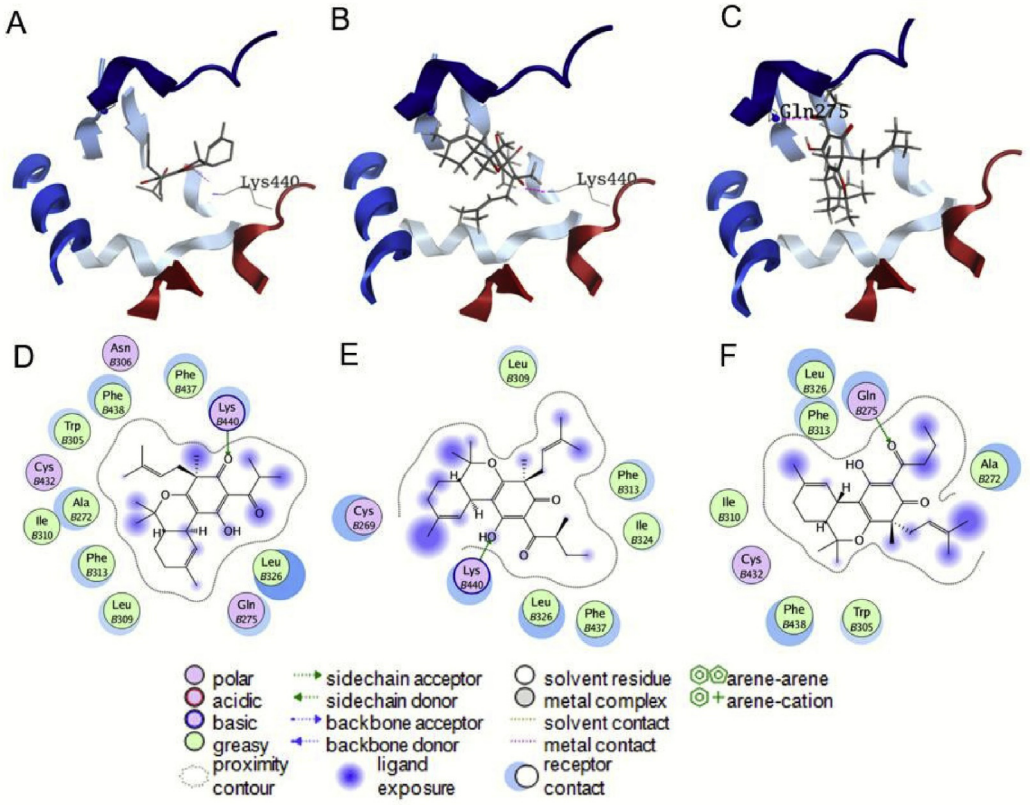

Fig. 9. Molecular docking of compounds 1–3 toward RXRα-LBD. (A) Docking of 1 to RXRα-LBD. (B) Docking of 2 to RXRα-LBD. (C) Docking of 3 to RXRα-LBD. (D) Binding site of 1 to the RXRα-LBD. (E) Binding site of 2 to the RXRα-LBD. (F) Binding site of 3 to the RXRα-LBD.

carbonyl group at C-6 of **1** and the hydroxyl group at C-2 of **2** could interact with Lys440 in the RXRα-LBD protein, while the carbonyl group at C-1′ of **3** could bind to the Gln275 of RXRα-LBD with a different interaction mode (Fig. 9). The predicted binding sites of **1–3** to RXRα-LBD were quite different from the traditional ligands which usually bind to Arg316 of the RXRα-LBD, such as for 9-*cis*-retinoic acid.

A preliminary SAR study was performed by extensive analysis of the structure and bioactivity. Compounds **1–3** possess the common monoterpenoid polyprenylated acylphloroglucinol skeleton with a 6/6/6 fused tricyclic system, while the only difference lies in the substituents at C-1′. Contrasting the activity results of compounds **1–3**, it was observed that **3**, with an *n*-propyl group at C-1′, showed more potent effects than compounds **1** and **2**, with an isopropyl group and a *sec*-butyl group at C-1′, respectively. Based on the above analysis, the *n*-propyl group at C-1′ in this type of compound is helpful for the RXRα related activities, which was confirmed by the molecular docking results in which **3** could bind to the Gln275 of the RXRα-LBD in a different interaction modes compared with **1** and **2**. Due to the limited quantities of the isolates, the thorough SAR needs further discussion.

3. Conclusion

In summary, three undescribed monoterpenoid polyprenylated acylphloroglucinols possessing a 6/6/6 fused tricyclic system, hyperelodiones A-C (**1–3**), were obtained from *H. elodeoides*. The monoterpenoid fragments in **1–3** were predicted to be biosynthesized by an isopentenyl at C-3 that formed a dihydropyran ring with the 4-OH of the core structure and another lateral prenyl group located at C-8 that cyclized into a six-membered ring by the carbon–carbon bond formation between C-5 and C-7. This was quite different from the reported monoterpenoid polyprenylated acylphloroglucinols, which were cyclized by a geranyl group (two prenyl groups linked from head to tail) at C-3. The phenomenon of keto-enol tautomerism existed in these monoterpenoid polyprenylated acylphloroglucinols. The major tautomer, with OH group at C-2, contributed in a high proportion and might due to the pseudo six-membered heterocyclic ring formed by

strong intramolecular hydrogen bonding between the active hydrogen and O-2′. The absolute configuration of **1** was assigned by the comparison of experimental and calculated ECD data, while the absolute configurations of **2** and **3** were assigned to be the same as **1** by their similar experimental ECD spectra and common biosynthetic origin. In addition, the putative biogenetic pathway of **1–3** was proposed. A fluorescence quenching assay suggested that **1–3** could bind to RXRα-LBD, whereas **3** showed the strongest interaction with a K_D of 12.81 μM. In addition, compounds **1–3** inhibited 9-*cis*-RA-induced RXRα transactivation and the growth of HeLa and MCF-7 cell lines in a dose-dependent manner, while **3** showed the most potent inhibitory activities. Western-blot assays showed dose-dependent PARP cleavage when HeLa cells and MCF-7 cells were exposed to **3**. Molecular docking results suggested that **3** with an *n*-propyl group could interact with the Gln275 moiety of RXRα-LBD, which was quite different from the interaction mode of **1** and **2**. Thus, **3** can be considered a promising lead compound for cancer therapy, which can bind to the RXRα-LBD and induce HeLa and MCF-7 cell apoptosis.

4. Experimental

4.1. General experimental procedures

Optical rotations were measured by using a Rudolph Autopol IV/IV-T polarimeter (NJ, USA). UV data were recorded on an UV-2600 UV/Vis spectrometer (Shimadzu, Japan). CD spectra were measured on a Chirascan spectropolarimeter (Applied Photophysics, UK). NMR spectra were conducted on a Bruker AVANCE III 600 MHz spectrometer (Bruker, Germany). High-resolution electrospray ionization mass spectra (HR-ESI-MS) were acquired by using a Thermo Fisher Q Exactive mass spectrometer (Thermo, USA). HPLC separations were performed with a Shimadzu LC-8A Liquid Chromatography system equipped with a DAD (Shimadzu, Japan). YMC (RP)-18 column (5 μm, 10 × 250 mm; YMC, Japan) were performed for reversed phase semipreparative separations. Silica gel (Qingdao Marine Chemical Ltd., China) and Sephadex LH-20 (Amersham Pharmacia Biotech, Sweden) were used for open column chromatography separations. Analytical thin-layer chromatography (TLC) separations were performed on silica gel GF254 plates (Qingdao Marine Chemical Inc., China).

4.2. Plant material

The whole plants of *Hypericum elodeoides* Choisy (wet) were collected from Ningde city, Fujian Province, China, in September 2016. They were authenticated by Prof. Zhen-Ji Li (College of the Environment & Ecology, Xiamen University). A voucher specimen (HE-201609) was deposited at the School of Pharmaceutical Sciences, Xiamen University.

4.3. Extraction and isolation

The dried and powdered whole plants of *H. elodeoides* (12.9 kg) were soaked overnight in 95% aqueous EtOH (4 × 100 L) at room temperature and then refluxed four times in 95% EtOH for 3 h each time. Concentration of the filtrate *in vacuo* to yielded the crude extract (949.7 g). The extract was suspended in water and partitioned consecutively with petroleum ether. The petroleum ether extract (150.7 g) was subjected to silica gel column chromatography (CC) eluted with a gradient of cyclohexane − EtOAc (1:0, 50:1, 25:1, 10:1, 5:1, 2:1, 1:1, 0:1) to afford eight fractions (Fr. a1 − Fr. a8). Fr. a3 (29.5 g) was further refined by silica gel CC eluted with petroleum ether − EtOAc (1:0, 400:1, 200:1, 100:1, 50:1, 25:1, 0:1) to afford eight fractions (Fr. a3A − Fr. a3H). Fr. a3E (9.9 g) was subsequently subjected to silica gel CC eluted with petroleum ether − acetone (200:1, 150:1, 100:1, 15:1, 0:1) to give six fractions (Fr. a3E1 − Fr. a3E6). Fr. a3E4 (5.8 g) was fractionated by silica gel CC eluted with cyclohexane − EtOAc (1:0, 1000:1, 500:1, 250:1, 100:1, 15:1, 0:1) to give five fractions (Fr. a3E4A − Fr. a3E4E). Finally, compound **2** (4.5 mg) was successfully separated by repeated prep-HPLC with MeOH–H_2O (97:3) at a flow rate of 5 mL/min, from Fr. a3E4C. Furthermore, Fr. a3E4D was purified by repeated prep-HPLC with 95% MeOH–H_2O at a flow rate of 5 mL/min, to yield compounds **1** (4.9 mg) and **3** (8.8 mg).

Hyperelodione A (**1**): yellowish oil; $[\alpha]_D^{28}$ –18.6 (*c* 0.43, CH_3OH); UV (CH_3OH) λ_{max} (log ε) 202 (4.06), 228 (3.98), 244 (4.00), 326 (3.82) nm; ECD (ACN) λ_{max} ($\Delta\varepsilon$) 198 (0.13), 239 (0.01), 313 (0.31) nm; IR (KBr)ν_{max} 3581, 2979, 2361, 1697, 1652, 1381, 1116, 974 cm^{-1}; ^1H and ^{13}C NMR data, see Table 1; HRESIMS m/z 413.2695 $[M+H]^+$ (cacld for $C_{26}H_{37}O_4$, 413.2686).

Hyperelodione B (**2**): yellowish oil; $[\alpha]_D^{28}$ +26.3 (*c* 0.35, CH_3OH); UV (CH_3OH) λ_{max} (log ε) 201 (3.78), 244 (3.74) nm; ECD (ACN) λ_{max} ($\Delta\varepsilon$) 198 (0.13), 237 (0.04), 313 (0.20) nm; IR (KBr)ν_{max} 3631, 2977, 2314, 1656, 1526, 1458, 1211, 1127 cm^{-1}; ^1H and ^{13}C NMR data, see Table 1; HRESIMS m/z 427.2846 $[M+H]^+$ (cacld for $C_{27}H_{39}O_4$, 427.2843).

Hyperelodione C (**3**): yellowish oil; $[\alpha]_D^{28}$ –23.0 (*c* 0.66, CH_3OH); UV (CH_3OH) λ_{max} (log ε) 201 (4.12), 227 (4.02), 243 (4.03), 324 (3.87) nm; ECD (ACN) λ_{max} ($\Delta\varepsilon$) 186 (−0.02), 243 (0.26), 322 (0.28) nm; IR (KBr)ν_{max} 3449, 2926, 2359, 1651, 1529, 1458, 1119 cm^{-1}; ^1H and ^{13}C NMR data, see Table 1; HRESIMS m/z 413.2678 $[M+H]^+$ (cacld for $C_{26}H_{37}O_4$, 413.2686).

4.4. RXRα-LBD purified protein

Human RXRα-LBD (223–462) was cloned as an N-terminal histidine-tagged fusion protein in the pET-15b vector and overexpressed in *E. coli* BL21 (DE3). After centrifugation, resuspension and sonication, the extract was incubated with the His60 Ni Superflow resin for 4 h. The combined protein was purified by a Ni2+-NTA agarose column at low temperatures.

4.5. Fluorescence measurements

Fluorescence measurements were performed on a Cary Eclipse Fluorescence spectrophotometer (Varian) in a 10 mm quartz cuvette. The 1 mM concentration of RXRα-LBD was incubated with different concentrations of compounds. The protein was excited at 280 nm and the fluorescence spectra between 290 nm and 500 nm were measured with the a spectrophotometer at RT. The data were analyzed by Origin 2017.

4.6. Luciferease report assay

First, 293T cells were transfected with plasmids combined with 10 μg/mL pGL5 luciferase reporter vector and 4 μg/mL pBIND- RXRα-LBD vector. After 12 h, cells were treated with different concentrations of compounds for 12 h and then lysed by PLB on an oscillating platform for 20 min. Firefly luciferase (FL) and Renilla luciferase (RL) activities were analyzed with the Dual-Luciferase Reporter Assay system (Promega).

Relative luciferase activity (%) = FL/RL × 100%

4.7. Cytotoxicity assay

HeLa cells and MCF-7 cells were seeded into 96-well plates at a density of 5 × 10^3 cells per well. After 12 h, cells were treated with different concentrations of compounds. After incubation for 48 h, 15 μL of MTT reagent and 60 μL of MEM (HeLa) or DMEM (MCF-7) was added and the cells were cultured for 4 h. After removing the supernatant, the transformed crystals were dissolved in DMSO (100 μL) and measured at 490 nm using a microplate reader (Thermo Multiskan MK3, Thermo Scientific, Helsinki, Finland). The cell proliferation-inhibition rate (%)

was calculated as follows:

Growth Rate (%)[(ODsample − ODblank)/(ODcontrol − ODblank)] × 100%

4.8. Western blotting

Equal amounts of the cell lysates were electrophoresed on a 10% SDS-PAGE gel and transferred to nitrocellulose. The membranes were blocked with 5% nonfat milk in TBST buffer (10 mM Tris–HCl [pH 8.0], 150 mM NaCl, and 0.05% Tween 20) at RT. After 1 h, the membranes were incubated with various primary antibodies at 4 ˚C overnight. After washing three times with TBST, the membranes were detected with either anti-mouse (1:3000) or anti-rabbit (1:3000) antibodies for 1 h and washed four times. The final immunoreactive products were visualized by using an enhanced chemiluminescence system.

4.9. Molecular docking studies

Molecular docking studies of compounds bound to RXRα-LBD were performed with MOE (2009.10) software. Compounds were imported into the MOE database in.sdf format which were further optimized via partial charge, energy minimization, and geometry optimization (Rebuild 3D) with a root-mean-square gradient of 0.01 and saved in the.mdb database format. The 3D structure of RXRα-LBD (https://doi.org/10.2210/pdb4zsh) was downloaded from the Research Collaboratory for Structural Bioinformatics Protein Data Bank (RCSB PDB). For the docking process, the “Triangle Matcher” placement method and London dG scoring function were selected, and the results were further refined by the force field method. Molecular docking simulations of compounds **1–3** with RXRα-LBD were conducted for 30 times, and the London dG scoring system was used to select the best interactions based on the smallest E_score2 provided.

Declaration of competing interest

The authors declare no competing financial interest.

Acknowledgments

This study was supported by the grants from National Natural Science Foundation of China (NSFC) (No.81602988), Fundamental Research Funds for the Central Universities (No.20720190079) the fund Education and scientific research project of Fujian Province (JAT160005) and Natural Science Foundation of Fujian Province of China (No.2019J007).

Appendix A. Supplementary data

Supplementary data to this article can be found online at https://doi.org/10.1016/j.phytochem.2019.112216.

References

Abe, I., Watanabe, T., Noguchi, H., 2004. Enzymatic formation of long-chain polyketid pyrones by plant type III polyketide synthases. Phytochemistry 65, 2447–2453. https://doi.org/10.1016/j.phytochem.2004.08.005.

Altucci, L., Leibowitz, M.D., Ogilvie, K.M., Lera, A.R., Gronemeyer, H., 2007. RAR and RXR modulation in cancer and metabolic disease. Nat. Rev. Drug Discov. 6, 793–810. https://doi.org/10.1038/nrd2397.

Ciochina, R., Grossman, R.B., 2006. Polycyclic polyprenylated acylphloroglucinols. Chem. Rev. 106, 3963–3986. https://doi.org/10.1021/cr0500582.

Decosterd, L.A., Stoeckli-Evans, H., Chapuis, J.C., Sordat, B., 1989. Hostettmann, K. New cell growth-inhibitory cyclohexadienone derivatives from *Hypericurn calycinurn* L. Helv. Chim. Acta 72, 1833–1845. https://doi.org/10.1002/hlca.19890720820.

Fobofou, S.A.T., Franke, K., Sanna, G., Prorzel, A., Bullita, E., Colla, P.L., Wessjohann, L.A., 2015. Isolation and anticancer, anthelminthic, and antiviral (HIV) activity of acylphloroglucinols, and regioselective synthesis of empetrifranzinans from *Hypericum roeperianum*. Bioorg. Med. Chem. Lett 23, 6327–6334. https://doi.org/10.1016/j.bmc.2015.08.028.

Hu, L.H., Sim, K.Y., Sampsoniones, A.-M., 2000. A unique family of caged polyprenylated benzoylphloroglucinol derivatives, from *Hypericum sampsonii*. Tetrahedron 56, 1379–1386. https://doi.org/10.1002/chin.200024231.

Lenhard, J.M., Lancaster, M.E., Paulik, M.A., Weiel, J.E., Binz, J.G., Sundseth, S.S., Gaskill, B.A., Lightfoot, R.M., Brown, H.R., 1999. The RXR agonist LG100268 causes hepatomegaly, improves glycaemic control and decreases cardiovascular risk and cachexia in diabetic mice suffering from pancreatic beta-cell dysfunction. Diabetologia 42, 545–554. https://doi.org/10.1007/s001250051193.

Li, Y.R., Xu, W.J., Wei, S.S., Lu, W.J., Lu, J., Kong, L.Y., 2019. Hyperbeanols F-Q, Diverse monoterpenoid polyprenylated acylphloroglucinols from the flowers of *Hypericum beanie*. Phytochemistry 159, 56–64. https://doi.org/10.1016/j.phytochem.2018.12.005.

Pei, Y.H., Li, X., Zu, T.R., 1989. An empirical correlations between optical rotation and absolute configuration of optical active α-methylbutyrylphloroglucinols and its synthesis. Acta Pharm. Sin. 24, 413–421.

Robinsonrechavi, M., Garcia, H.E., Laudet, V., 2003. The nuclear receptor superfamily. J. Cell Sci. 116, 585–586. https://doi.org/10.1242/jcs.00247.

Tian, W.J., Qiu, Y.Q., Chen, H.F., Jin, X.J., Yao, X.J., Dai, Y., Yao, X.S., 2017a. Chiral separation and absolute configurations of two pairs of racemic polyprenylated benzophenones from *Hypericum sampsonii*. Fitoterapia 116, 39–44. https://doi.org/10.1016/j.fitote.2016.10.014.

Tian, W.J., Qiu, Y.Q., Chen, J.J., Yao, X.J., Wang, G.H., Dai, Y., Chen, H.F., Yao, X.S., 2017b. Norsampsone E, an unprecedented decarbonyl polycyclic polyprenylated acylphloroglucinol with a homoadamantyl core from *Hypericum sampsonii*. RSC Adv. 53, 33113–33119. https://doi.org/10.1039/c7ra05947g.

Tian, W.J., Qiu, Y.Q., Jin, X.J., Chen, H.F., Yao, X.J., Dai, Y., Yao, X.S., 2016. Hypersampsones S–W, new polycyclic polyprenylated acylphloroglucinols from *Hypericum sampsonii*. RSC Adv. 6, 50887–50894. https://doi.org/10.1039/c5ra26332h.

Tian, W.J., Qiu, Y.Q., Jin, X.J., Chen, H.F., Yao, X.J., Dai, Y., Yao, X.S., 2014a. Novel polycyclic polyprenylated acylphloroglucinols from *Hypericum sampsonii*. Tetrahedron 70, 7912–7916. https://doi.org/10.1055/s-0034-1382626.

Tian, W.J., Qiu, Y.Q., Yao, X.J., Chen, H.F., Dai, Y., Zhang, X.K., Yao, X.S., 2014b. Dioxasampsones A and B, two polycyclic polyprenylated acylphloroglucinols with unusual epoxy-ring-fused skeleton from *Hypericum sampsonii*. Org. Lett. 16, 6346–6349. https://doi.org/10.1021/ol503122m.

Tian, W.J., Yu, Y., Yao, X.J., Chen, H.F., Dai, Y., Zhang, X.K., Yao, X.S., 2014c. Norsampsones A-D, four new decarbonyl polycylic polyprenylated acylphloroglucinols from *Hypericum sampsonii*. Org. Lett. 16, 3448–3451. https://doi.org/10.1039/c7ra05947g.

Yang, X.W., Grossman, R.B., Xu, G., 2018. Research progress of polycyclic polyprenylated acylphloroglucinols. Chem. Rev. 118, 3508–3558. https://doi.org/10.1021/acs.chemrev.7b00551.

Yang, X.W., Li, M.M., Liu, X., Ferreira, D., Ding, Y., Zhang, J.J., Liao, Y., Qin, H.B., Xu, G., 2015. Polycyclic polyprenylated acylphloroglucinol congeners possessing diverse structures from *Hypericum henryi*. J. Nat. Prod. 78, 885–895. https://doi.org/10.1021/acs.jnatprod.5b00057.

Yang, X.W., Li, Y.P., Su, J., Ma, W.G., Xu, G., 2016. Hyperjapones A−E, terpenoid polymethylated acylphloroglucinols from *Hypericum japonicum*. Org. Lett. 18, 1876–1879. https://doi.org/10.1021/acs.orglett.6b00650.

Zhang, J.J., Yang, X.W., Ma, J.Z., Ye, Y., Shen, X.L., Xu, G., 2015. Cytotoxic polyprenylated acylphloroglucinol derivatives from *Hypericum henryi*. Tetrahedron 71, 8315–8319. https://doi.org/10.1016/j.tet.2015.08.059.

Zhu, H., Chen, C., Liu, J., Sun, B., Wei, G.Z., Li, Y., Zhang, J., Yao, G., Luo, Z.W., Xue, Y.B., Zhang, Y.H., 2015. Hyperascyrones A–H, polyprenylated spirocyclic acylphloroglucinol derivatives from *Hypericum ascyron* Linn. Phytochemistry 115, 222–230. https://doi.org/10.1016/j.phytochem.2015.02.009.